Available online at www.sciencedirect.com

SciVerse ScienceDirect

Ceramics International 39 (2013) 6369–6377

CERAMICS INTERNATIONAL

www.elsevier.com/locate/ceramint

Defect chemistry of a high-k 'Y5V' $(Ba_{0.95}Eu_{0.05})TiO_3$ ceramic

Da-Yong Lu[a,*], Li Zhang[a,b], Xiu-Yun Sun[a]

[a]Research Center for Materials Science and Engineering, Jilin Institute of Chemical Technology, Jilin 132022, China
[b]College of Chemistry, Northeast Normal University, Changchun 130024, China

Received 20 November 2012; received in revised form 15 January 2013; accepted 21 January 2013
Available online 29 January 2013

Abstract

The influence of the sintering temperature (T_s) on the structure, dielectric and valence-state properties of $(Ba_{1-x}Eu_x)TiO_3$ ($x=0.05$) ceramics was investigated using X-ray diffraction (XRD), scanning electron microscopy (SEM), electron paramagnetic resonance (EPR), Raman spectroscopy, and dielectric temperature measurements. An increase in T_s can increase the solubility limit of Eu in $BaTiO_3$. When the T_s was increased to 1450 °C, a high-k 'Y5V' ($\varepsilon'_{RT}=8500$) ceramic (C-BE5T) with a single-phase cubic structure was obtained. The dielectric peak shifted rapidly toward lower temperatures with increasing T_s at a rate of −0.46 °C/K. A symmetric (200) XRD peak, exaggerated grain growth (5.6 μm), a mixed valence of Eu^{2+}/Eu^{3+}, an asymmetric main Raman band at 2494 cm^{-1} and a weak sharp band at 1516 cm^{-1} in the high-wavenumber region are characteristics of cubic symmetry of C-BE5T. The formation of a solid solution of C-BE5T and defect chemistry are discussed.

Keywords: A. Powders: solid state reaction and Sintering; B. Defects; C. Dielectric properties; D. BaTiO3 and titanates

1. Introduction

Europium-doped barium titanate ($BaTiO_3$) ceramics or powders have drawn a great deal of attention because of their luminescence properties [1–4]. In 2005, however, a low-porosity, highly-insulating, dielectric-ageing-resistant, and fine-grained $(Ba_{1-x}Eu_x)Ti_{1-x/8}O_3$ ($x=0.05$) ceramic that exhibited dielectric-temperature stability in a lower temperature range of −100 to 50 °C was obtained, accompanied by the appearance of a secondary phase, $Eu_2Ti_2O_7$, which was formed due to the solubility limit of $x=0.03$ at a powder sintering temperature of 1300 °C [5]. Since then, the valence state and site occupation of Eu ions in the $BaTiO_3$ lattice and the dielectric properties associated with different charge-compensation mechanisms have been successively investigated [6–10]. Europium may occupy Ba sites as Eu^{3+} [6–8] or as mixed Eu^{3+}/Eu^{2+} [6,9], or may occupy both Ba and Ti sites as Eu^{3+} [9,10]. Eu has been reported to prefer Ba sites to Ti sites but can transfer from Ba sites to Ti sites depending on the Ba/Ti ratio [10]. Electron paramagnetic resonance (EPR) investigations suggested that a self-compensation mode with the amphoteric behavior of Eu ions can occur in $(Ba_{1-x/2}Eu_{x/2})(Ti_{1-x/2}Eu_{x/2})O_3$ ($x=0.05$) and results in no reduction of Eu^{3+} to Eu^{2+} occurring [9]. For $(Ba_{1-x}Eu_x)TiO_3$ ceramics prepared via a solid-state method, however, no evidence for the valence change of Eu^{3+} to Eu^{2+} was provided [8]. Eu-doped $BaTiO_3$ generally exhibits a tetragonal structure and its dielectric peak cannot reach room temperature because of the solubility limit of $x=0.03$ [5]. A single-phase and high-k 'Y5V' $(Ba_{1-x}Eu_x)TiO_3$ ($x\le 0.05$) has not been reported to date. (*Note*: Y5V specification: $-82\% \le (\varepsilon'-\varepsilon'_{RT})/\varepsilon'_{RT} \le +22\%$ in a temperature range of −30 to 85 °C)

In this work, $(Ba_{1-x}Eu_x)TiO_3$ ($x=0.05$) ceramics were prepared at different sintering temperatures (T_s) using a cold-pressing ceramic technique. Our objective is to increase the T_s to increase the solubility limit of Eu in $BaTiO_3$ to obtain a single-phase cubic ceramic and realize a high-k Y5V behavior. The structural, dielectric and valence-state properties of the

*Corresponding author. Tel.: +86 13944220469.
E-mail addresses: cninjp11232000@yahoo.com, dylu@jlict.edu.cn (D.-Y. Lu).

0272-8842/$ - see front matter © 2013 Elsevier Ltd and Techna Group S.r.l. All rights reserved.
http://dx.doi.org/10.1016/j.ceramint.2013.01.063

cubic $(Ba_{1-x}Eu_x)TiO_3$ ceramic were investigated using XRD, SEM, ESR, Raman spectroscopy, and dielectric measurements to elucidate the solid solution formation and the defect chemistry. The high-wavenumber Raman and EPR spectra in the cubic phase showed novel features.

2. Experimental procedures

$(Ba_{1-x}Eu_x)TiO_3$ ($x=0.05$) ceramics (abbreviated BE5T) were prepared using a cold-pressing ceramic technique described elsewhere [5]. The final sintering conditions were chosen as 1200, 1250, 1300, 1350, 1400, and 1450 °C for 3 h. $Eu_2Ti_2O_7$ and Eu_2O_3 ceramics were prepared at 1300 °C under the same route as that used for BE5T for Raman scattering analyses and comparison. Powder X-ray diffraction (XRD) measurements were performed between $20° \le 2\theta \le 100°$ in steps of 0.02° using a DX-2700 X-ray diffractometer (Dandong Haoyuan Inc.). Lattice parameters and unit cell volume were calculated by MS Modeling software package (Accelrys Inc.) using Cu Kα1 radiation ($\lambda=1.540562$ Å). Scanning electric microscopy (SEM) images were obtained using a JSM-6490 SEM (JEOL) operated at 25 kV. The temperature dependence of the dielectric permittivity and loss was measured from −75 to 200 °C with a weak 1 kHz ac electric field using an RCL meter (Fluke PM6306). Electron paramagnetic resonance (EPR) spectra were measured at an X-band frequency of 9.148 GHz from 25 to 150 °C in the sweep range of 50–550 mT using a JES-RE3X spectrometer (JEOL) equipped with a Mn^{2+} standard marker. The gyromagnetic values (g values) were calculated in terms of the third and fourth lines of the Mn^{2+} standard sextet marker ($g_3=2.0327$ and $g_4=1.9810$). Raman spectra of the ceramic powders were measured at room temperature using a LabRAM XploRA Raman spectrometer (Horiba Jobin Yvon), with a 532 nm laser focused on a spot of approximately 3–5 μm in diameter. The Raman spectrometer was equipped with a Linkam-600 heating and cooling stage for temperature-dependent Raman measurements from −150 to 180 °C.

3. Results

Powder XRD patterns of all the BE5T ceramics sintered at different sintering temperatures (T_s) are shown in Fig. 1. The main perovskite phase was formed at each T_s. When the T_s was less than 1400 °C, a small amount of a second phase separated from the main tetragonal perovskite phase. A pyrochlore phase, $Eu_2Ti_2O_7$ (JCPDS: no. 23-1072), appeared at $T_s=1250$ °C and the quantity of this phase gradually decreased with increasing T_s. For the main tetragonal perovskite phase, the separate (002) and (200) peaks shift toward each as T_s is increased, as shown in Fig. 2. This shift indicates a decrease in tetragonality. When the T_s was increased to 1450 °C, the $Eu_2Ti_2O_7$ phase disappeared and a single-phase ceramic formed, with a symmetric (200) peak characteristic of a cubic structure.

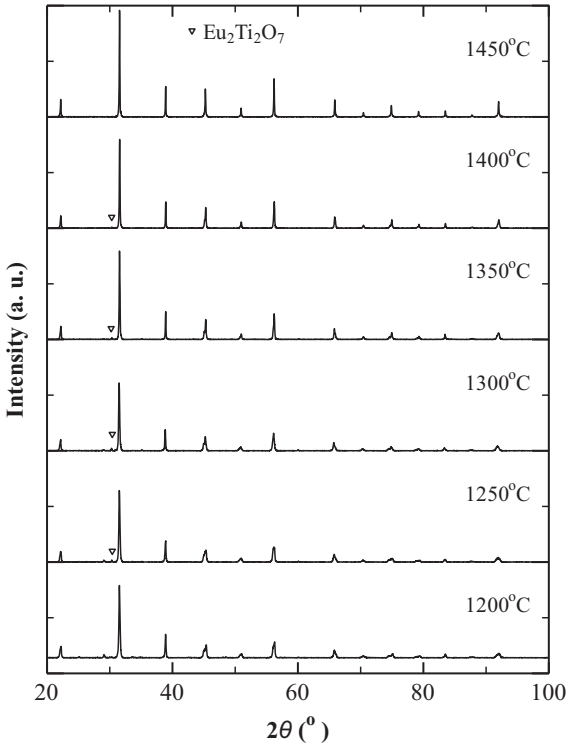

Fig. 1. XRD patterns of BE5T ceramics prepared at different sintering temperatures ($T_s=1250$–1450 °C).

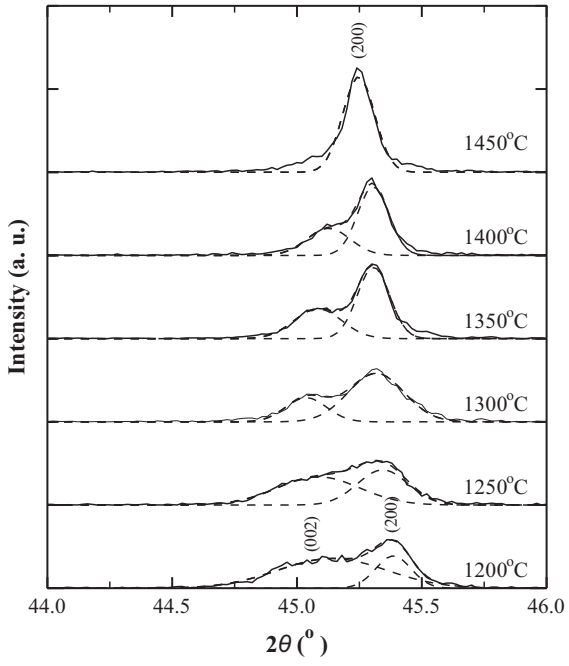

Fig. 2. Gaussian fitting of the XRD peaks in the vicinity of 45° in Fig. 1.

The unit-cell volume (V_0) of the cubic BE5T sample (called C-BE5T in the following) was determined to be 64.31 Å^3, which is significantly less than the V_0 (65.50 Å^3) of the cubic $BaTiO_3$ (JCPDS: no. 31–174). C-BE5T can therefore be considered as a sufficient incorporation of Eu ions into Ba sites in the $BaTiO_3$ lattice; otherwise, an expansion of the crystal cells would be observed if Eu entered the Ti sites

as Eu^{3+} [9]. An increase in T_s from 1300 to 1450 °C resulted in an increase in the solubility limit of Eu ions in $BaTiO_3$ from $x=0.03$ [5] to 0.05.

The grains in BE5T grew rapidly with increasing T_s, as shown in the SEM observations in Fig. 3. BE5T exhibited a high porosity when $T_s \leq 1300$ °C. In the T_s range of 1250–1400 °C, BE5T became denser and exhibited medium-sized grains (1.5–2.6 μm) and a homogeneous grain size distribution. A striking grain growth ($g=5.6$ μm) and closest sintering behavior occurred in C-BE5T sintered at 1450 °C (Fig. 4).

The temperature dependences of the dielectric permittivity (ε') and the dielectric loss (tan δ) for BE5T are shown in Fig. 5(a) and (b). The dielectric-temperature characteristics of BE5T exhibited a diffuse phase transition (DPT) behavior. The maximum permittivity (ε'_m) increased with increasing T_s (Fig. 5(a)). The dielectric-peak temperature (T_m) decreased linearly with T_s at a rate of −0.46 °C/K, as shown in the inset in Fig. 5(a). For C-BE5T, the ε'_m was as high as 9000 at $T_m=19$ °C and its room-temperature permittivity (ε'_{RT}) was 8500. The high-k Y5V dielectric specification can be realized in C-BE5T. The tan δ value of all the BE5T ceramics were significantly lower (<0.03) at temperatures less than 140 °C (Fig. 5(b)).

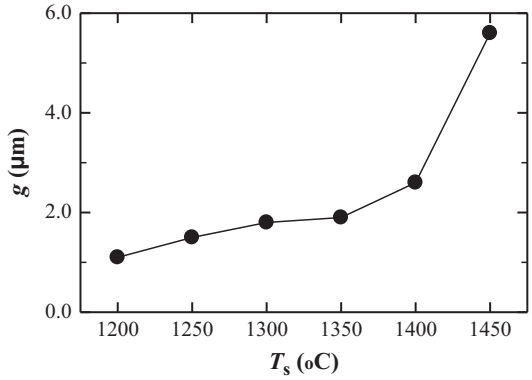

Fig. 4. Variation in the average grain size (g) as a function of T_s for BE5T.

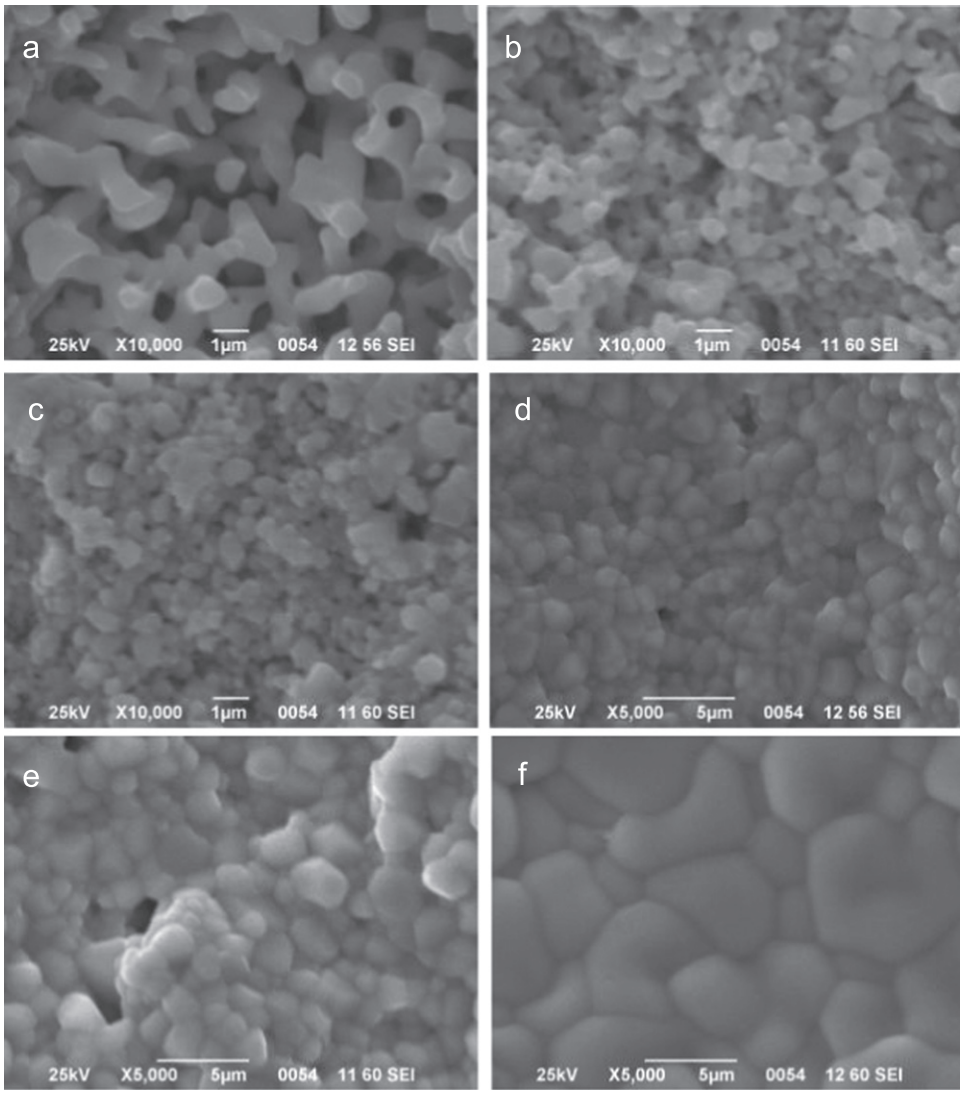

Fig. 3. SEM images for BE5T ceramics sintered at (a) 1200 °C, (b) 1250 °C, (c) 1300 °C, (d) 1350 °C, (e) 1400 °C and (f) 1450 °C.

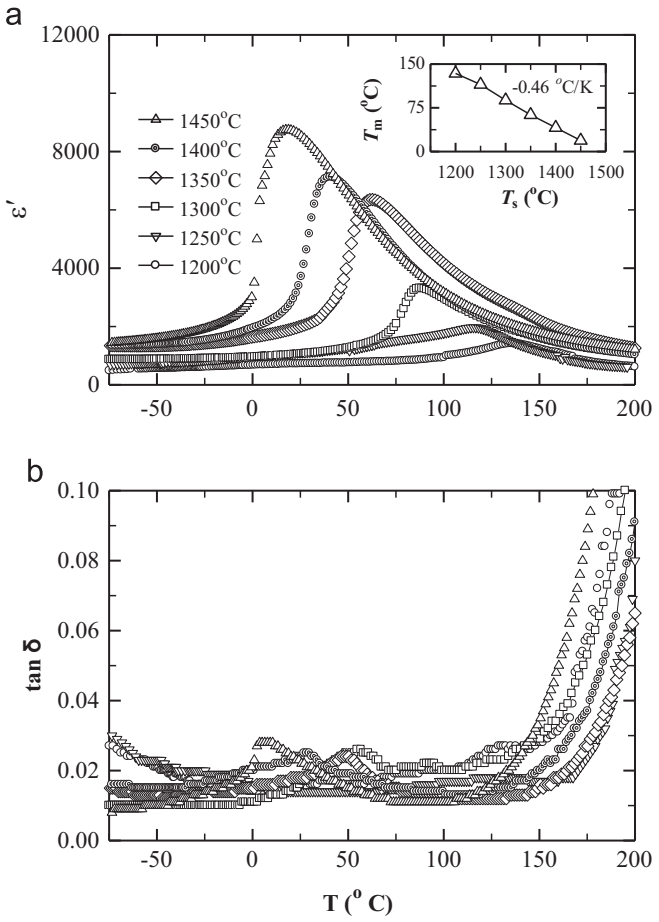

Fig. 5. Temperature dependences of (a) the dielectric permittivity (ε') and (b) the dielectric loss ($\tan\delta$) for BE5T. The inset depicts the change in dielectric-peak temperature (T_m) with increasing T_s.

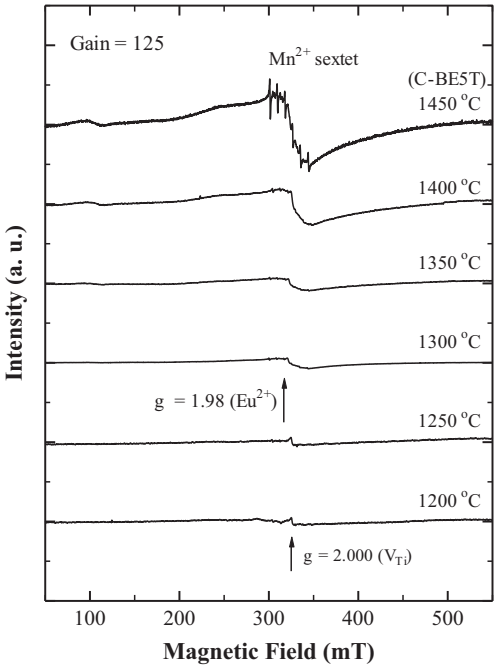

Fig. 6. Room-temperature EPR spectra of BE5T ceramics sintered at T_s (1250–1450 °C).

Room-temperature EPR spectra of BE5T are shown in Fig. 6. When $T_s \leq 1400$ °C, a signal with $g=2.000$ was observed and was synchronous with the appearance of $Eu_2Ti_2O_7$ in BE5T. This signal is associated with Ti-vacancy defects (V_{Ti}) [9,11–13] induced by Eu^{3+} ions at Ba sites.

Eu^{2+} appeared at $T_s \geq 1300$ °C because a broad $g=1.98$ signal is the signature of Eu^{2+} ($4f^7$) in the $BaTiO_3$ lattice [6,9]. The line intensity of this signal increased with T_s, which indicates that an increase in T_s can contribute to the conversion of Ba-site Eu^{3+} into Eu^{2+}. No Eu^{2+} was detected by EPR at $T_s \leq 1250$ °C. This result implies that a mixed valence of Eu^{3+}/Eu^{2+} exists in the BE5T ceramics sintered at $T_s \geq 1300$ °C on the basis of the evolution of the $g=1.98$ signal.

Mn impurities usually exist in $BaTiO_3$ ceramics [9,14]. The Mn^{2+} ($3d^5$) sextet signal was very weak when $T_s \leq 1400$ °C (Fig. 6). However, a strong Mn^{2+} signal was observed in C-BE5T, which indicates that a large number of Mn^{4+} or Mn^{3+} impurities in C-BE5T were reduced into Mn^{2+}.

The $g=2.000$ signal related to Ba-site Eu^{3+} is sensitive to the tetragonal-cubic phase transition. This signal is weaker in the tetragonal phase, whereas it is clearly visible in the cubic phase [6,9,13]. To investigate whether Eu^{3+} exists in C-BE5T, EPR signals for all BE5T samples were measured at different measuring temperatures (T), as shown in Fig. 7. The $g=2.000$ signal of BE5T was activated markedly at 150 °C above each T_m when $T_s \leq 1400$ °C. This fact suggests that Eu^{3+} exists in BE5T samples sintered at $T_s \leq 1400$ °C. However, no signal at $g=2.000$ was observed for C-BE5T, which implies that almost all of the Eu ions exist as Eu^{2+} in C-BE5T.

Room-temperature Raman spectra of the BE5T ceramic powders are shown in Fig. 8(a) and (b). It is well known that the tetragonal $BaTiO_3$ in the low-wavenumber region of 100–1200 cm^{-1} shows the four phonon modes that peak at approximately 260 cm^{-1} [A_1 (TO_2)], 520 cm^{-1} [A_1 (TO_3)], 720 cm^{-1} [A_1 (LO_3)+E (LO_3)], and 305 cm^{-1} [B_1+E(TO+LO)] [15]. The first three modes appeared in all the BE5T samples. A band at 308 cm^{-1} is an indication of tetragonality for $T_s \leq 1400$ °C. As evident from the spectra in Fig. 8(a), the intensity of the 308 cm^{-1} band decreased as the T_s was increased, which indicates a decrease in tetragonality. This result is in good agreement with the XRD results. The 308 cm^{-1} band disappeared in C-BE5T with cubic symmetry.

A band at 840 cm^{-1} appeared in BE5T. We attributed this band to an internal deformation of the BO_6 octahedron caused by the charge difference of different types of ions (Eu^{3+}) at equivalent sites (Ba^{2+}) in the $BaTiO_3$ lattice [9,15]. The intensity of this band may be considered as an indication of the amount of Eu^{3+} ions incorporated into the $BaTiO_3$ lattice [16]. The Eu^{3+} content increased with T_s until 1400 °C (Fig. 8(a)). It was found that the equivalent substitution of divalent ions, such as Sr^{2+} [17] and Ca^{2+} [18] at Ba sites,

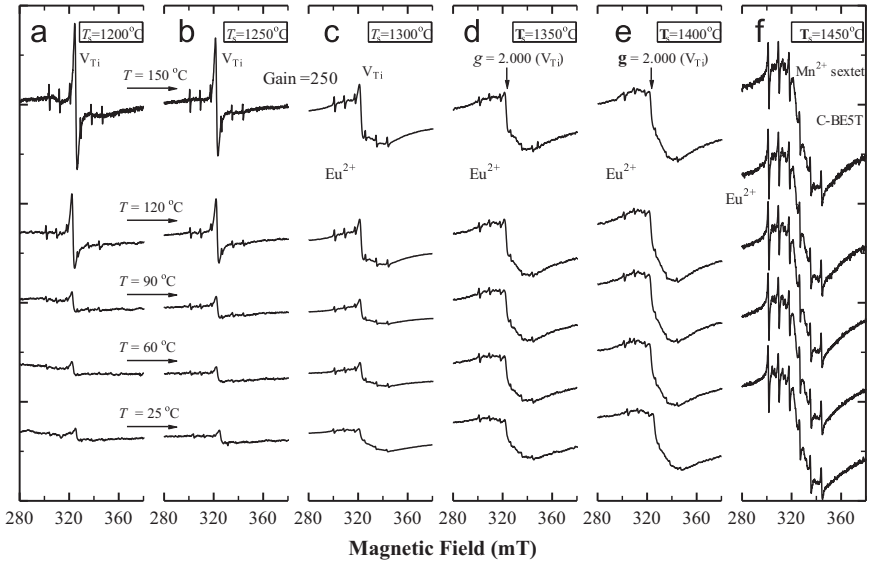

Fig. 7. Evolution in EPR signals as a function of temperature for BE5T ceramics sintered at (a) 1200 °C, (b) 1250 °C, (c) 1300 °C, (d) 1350 °C, (e) 1400 °C and (f) 1450 °C.

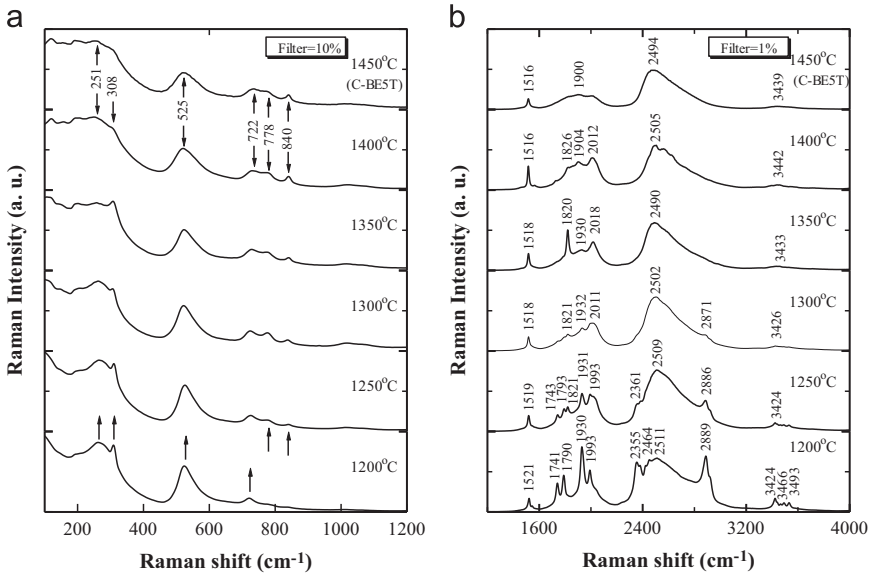

Fig. 8. Room-temperature Raman spectra of BE5T ceramics sintered at different temperatures, measured in (a) the low-wavenumber region of 100–1200 cm^{-1} and (b) the high-wavenumber region of 1200–4000 cm^{-1}.

could not cause Raman activity at 840 cm^{-1}. A reasonable assumption was made that Ba-site Eu^{2+} would not induce the 840 cm^{-1} band. The 840 cm^{-1} line intensity of C-BE5T was so high that its intensity was not lower than that observed in BE5T sintered at 1400 °C and in La-doped $BaTiO_3$ ceramics [15,16], which suggests that almost all of the Eu ions exist as Eu^{3+} in C-BE5T. This conclusion is contrary to that based on the EPR results, i.e, that Eu ions exist as Eu^{2+} in C-BE5T. This contradiction will be discussed further in the Section 4.

An additional band at 778 cm^{-1} appeared when $T_s \geq 1250$ °C. Lazarevic et al. observed this band in undoped $BaTiO_3$ and attributed it to a multiphonon (305 cm^{-1} + 453 cm^{-1}) [19]. This band was also observed in $Ba(Ti_{1-x}Zr_x)O_3$ [20–22]. We assign the 778 cm^{-1} band to a multiphonon (250 cm^{-1} + 525 cm^{-1}) here for the two reasons: (1) the 778 cm^{-1} band also appeared in the spectrum of C-BE5T, which exhibits a cubic structure, and the 308 cm^{-1} band did not appear in the spectrum of C-BE5T; and (2) the 453 cm^{-1} optical mode [E (TO_3) + E (LO_2)] is weak-swelling [15], which means it is not sufficiently strong to induce such an band at 778 cm^{-1} through overlap of the 308 cm^{-1} band.

An interesting phenomenon observed for BE5T is that several strong bands appear in the high-wavenumber region of 1200–4000 cm^{-1} (Fig. 8(b)) and that the intensities of these bands are approximately 10 times greater than those observed in the low-wavenumber region of

100–1200 cm^{-1}. We have never observed these bands in the spectra of other rare-earth-doped $BaTiO_3$ samples. The spectrum of C-BE5T shows a weaker sharp band, two broad and strong bands, and a weak band, with peaks at 1516, 1900, 2494, and 3439 cm^{-1}, respectively.

Because BE5T sintered at $T_s \leq 1400$ °C contains $Eu_2Ti_2O_7$ and possible Eu_2O_3, the room-temperature Raman spectra of $Eu_2Ti_2O_7$ and Eu_2O_3 ceramics were measured, as shown in Fig. 9(a) and (b), which includes the Raman spectra of C-BE5T for comparison. The Eu_2O_3 showed astonishing Raman activity; its line intensity at 2743 cm^{-1} was 700 times greater than that of the main band at 250 cm^{-1} in the perovskite phase. The intensities in the high-wavenumber Raman spectrum of $Eu_2Ti_2O_7$ were weaker. The comparison in Fig. 9 verifies that, when the T_s is increased to 1450 °C, both $Eu_2Ti_2O_7$ and the starting material Eu_2O_3 were completely incorporated into the lattice to form a single-phase C-BE5T. The four high-wavenumber bands may represent the structural nature of C-BE5T. For the two tetragonal BE5T ceramics sintered at 1350 and 1400 °C, the bands at 1900 and 2494 cm^{-1} consisted of three and two peaks, respectively (Fig. 8(b)). In fact, the 1900 cm^{-1} broad band of C-BE5T also showed a three-peak nature.

The temperature-dependent Raman spectra of C-BE5T are shown in Fig. 10. Similar to two other bands at 250 and 520 cm^{-1} in the spectrum of C-BE5T, the multi-phonon mode at 778 cm^{-1} and the band at 840 cm^{-1} persist beyond T_m (=19 °C) (Fig. 10(a)) and are attributed to disorder in the cubic phase. The evolution of Raman spectra in the high-wavenumber region shows two features (Fig. 10(b)): (1) when the measuring temperature (T) was lower than T_m, C-BE5T could be considered as entering the ferroelectric phase. The sharp band at 1516 cm^{-1} exhibited a high intensity. (2) When $T > T_m$, this sharp band attenuated rapidly. The main band at 2494 cm^{-1} exhibited an asymmetric unimodal pattern and its intensity decreased with increasing T. When T decreased below T_m, this band split into two peaks ($-30 \leq T \leq 0$ °C) and further into three peaks ($T \leq -60$ °C). Thus, in addition to the disappearance of the 308 cm^{-1} band that indicates tetragonality, an asymmetric main band at 2494 cm^{-1} and a weaker sharp band at 1516 cm^{-1} in C-BE5T can also be considered indications of cubic symmetry.

4. Discussion

4.1. Solid solution formation of C-BE5T

C-BE5T [$(Ba_{1-x}Eu_x)TiO_3$ (x=0.05)] sintered at 1450 °C is a single-phase ceramic with a cubic perovskite structure. Europium would exist as metastable Eu^{2+} if Ti ions were relatively stable in their 4+ oxidation state. A broad EPR signal at g=1.98 verified that Ba-site Eu exists predominantly as Eu^{2+} in C-BE5T. However, the existence of the 840 cm^{-1} Raman band leads to the opposite conclusion, i.e., that Eu exists as Eu^{3+} in C-BE5T. These two conclusions obviously contradict each other. We understand and resolve this contradiction in terms of the analysis of the formation of a solid solution of BE5T.

When T_s=1250 °C, Eu ions as Eu^{3+} are incorporated into the perovskite lattice to induce Ti-vacancy (V_{Ti}) defects, and a small amount of a $Eu_2Ti_2O_7$ phase appears:

$$2Eu_2O_3 + 3TiO_2 \rightarrow 4Eu_{Ba}^{3+} + 3Ti_{Ti}^{4+} + 12O_O^{2-} + V_{Ti} \quad (1)$$

The maximum concentration of Ti vacancies is 1.25% in BE5T if all of Eu ions (x=0.05) exist as Eu^{3+} in the perovskite lattice. The solubility limit is x=0.03 at T_s=1300 °C [5], which means that the ratio of Eu^{3+} to Eu in BE5T is not less than 60%, whereas that in $Eu_2Ti_2O_7$ is approximately 40%, which corresponds to x=0.02.

The sintering effect of the cold-pressing ceramic technique at higher temperatures ($T_s \geq 1300$ °C) is similar to that of the solid-state reaction under high pressure and at a lower temperature (4.0 GPa, 1090 °C) [23]. High-temperature sintering in air can reduce a certain amount of Ti^{4+} ions to Ti^{3+} ions and partially decompose the $Eu_2Ti_2O_7$ phase into

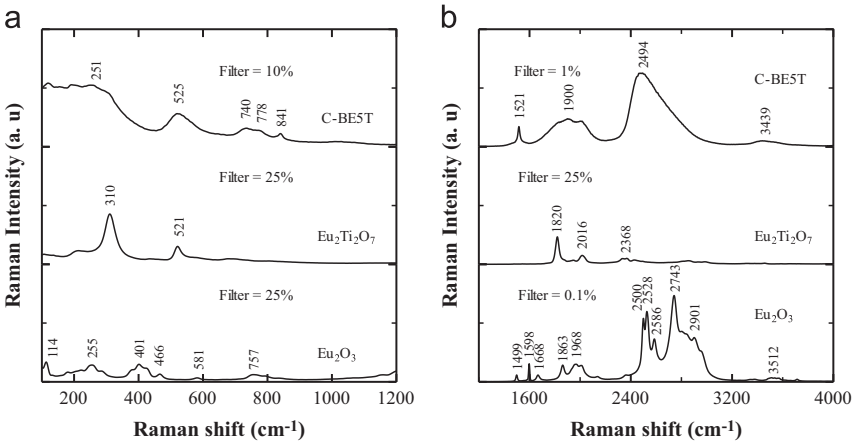

Fig. 9. Room-temperature Raman spectra of $Eu_2Ti_2O_7$, Eu_2O_3 ceramics, and C-BE5T, measured in (a) the low-wavenumber region of 100–1200 cm^{-1} and (b) the high-wavenumber region of 1200–4000 cm^{-1}.

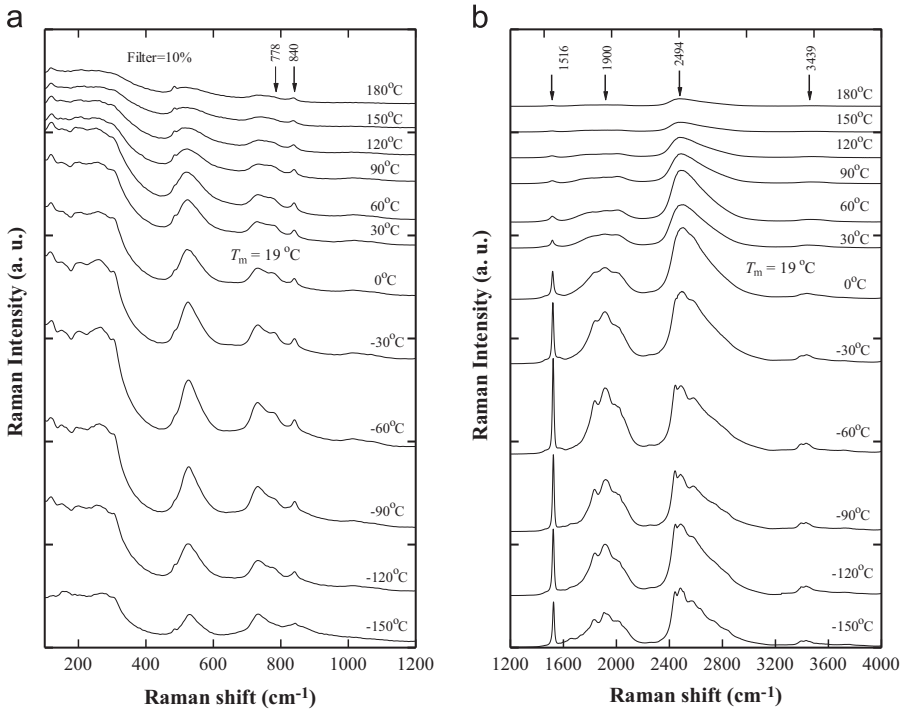

Fig. 10. Temperature-dependent Raman spectra of C-BE5T, measured in (a) the low-wavenumber region of 100–1200 cm^{-1} and (b) the high-wavenumber region of 1200–4000 cm^{-1}.

lattice ions:

$$2Eu_2Ti_2O_7 \rightarrow 4Eu_{Ba}^{3+} + 4Ti_{Ti}^{4+} + 12O_O^{2-} + O_2\uparrow \quad (2)$$

One Ti^{3+} ion can concatenate one Eu^{3+} ion to form a Ti^{3+}–Eu^{3+} defect complex incorporated in its entirety into the perovskite lattice. The instability of Ti^{3+} (Eq. (3)) can indirectly convert Eu^{3+} into metastable Eu^{2+} (Eq. (4)) to maintain a dynamic equilibrium expressed by Eq. (5).

$$Ti_{Ti}^{3+} \leftrightarrow Ti_{Ba}^{4+} + e \quad (3)$$

$$Eu_{Ba}^{3+} + e \leftrightarrow Eu_{Ba}^{2+} \quad (4)$$

$$Eu_{Ba}^{3+} + Ti_{Ti}^{3+} \leftrightarrow Eu_{Ba}^{2+} + Ti_{Ti}^{4+} \quad (5)$$

A stronger Eu^{2+} signal in BE5T sintered at T_s=1300 °C was detected (Figs. 6 and 7). This stronger signal implies that the conversion of Eu^{3+} to Eu^{2+} (Eqs. (4) and (5)) occurred at this temperature. This conversion will reduce the Ti-vacancy concentration and increase the solid solubility of $Eu_2Ti_2O_7$ into the perovskite lattice.

As T_s is increased, the internal conversion of Eu^{3+} to Eu^{2+} becomes more active; consequently, the Ti^{3+} concentration in Eq. (5) increases, and the concentration of the $Eu_2Ti_2O_7$ phase gradually decreases. When the T_s is increased to 1450 °C, the Ti^{3+} concentration is sufficiently high to be able to concatenate all Eu^{3+} ions (x=0.02, i.e. Eu^{3+}/Eu=40%) in the residual $Eu_2Ti_2O_7$ phase, which is then completely incorporated into the perovskite lattice. The Ti vacancies (V_{Ti}) also disappear due to the increase in convertibility of Eu^{3+} to Eu^{2+} as T_s is increased. The instable Ti^{3+} and metastable Eu^{2+} can be stabilized by the dynamic equilibrium (Eq. (5)). A single-phase solid solution of C-BE5T is formed and is relatively stable.

An EPR signal with g=1.9612 is associated with Ti^{3+} ($3d^1$) in $BaTiO_3$ [24]. However, the nature of this signal is still under debate [24]. This signal was not detected in C-BE5T, which is most likely because Ti ions tend to be observed as Ti^{4+} ($3d^0$) ions because of the dynamic equilibrium or because the Ti^{3+} signal is too weak to be observed relative to the Eu^{2+} and Mn^{2+} signals.

4.2. Defect chemistry of C-BE5T

The defect chemistry of C-BE5T is closely related to the above solid solution formation. In C-BE5T, the defects are Eu^{3+}, metastable Eu^{2+} at Ba sites and Ti^{3+} at Ti sites. O-vacancy defects can be ruled out owing to high insulation ($>10^8$ Ωm) and a much lower dielectric loss. The molecule can be expressed by $(Ba_{1-x}^{2+}Eu_{x-\delta}^{2+}Eu_{\delta}^{3+})(Ti_{1-\delta}^{4+}Ti_{\delta}^{3+})O_3$. The compensation mode can be described by the dynamic equilibrium in Eq. (5). The self-compensation mode [9] can be not formed owing to the limit of (Ba+Eu)/Ti=1.

Europium ions in C-BE5T exhibit a dual character of both Eu^{2+} and Eu^{3+} because of the dynamic charge equilibrium. Hence, the opposite conclusions drawn with respect to observations related to Eu^{2+} and Eu^{3+} based on the EPR and Raman results does not create a contradiction.

The ε'-T curve of C-BE5T exhibits a high-k Y5V behavior because DPT occurs at approximately room temperature. A dipolar nano-domain (or order-disorder)

mode [25] is responsible for DPT in C-BE5T, as evidenced by its Raman response.

As intrinsic defects, a large number of Mn^{4+} or Mn^{3+} impurities in C-BE5T can trap electrons in the dynamic equilibrium to be reduced into Mn^{2+}, i.e., $Mn_{Ti}^{4+}+2e\rightarrow Mn_{Ti}^{2+}$ or $Mn_{Ti}^{3+}+e\rightarrow Mn_{Ti}^{2+}$. As a result, a strong Mn^{2+} sextet signal was observed. The reduction of Mn^{4+} or Mn^{3+} to Mn^{2+} greatly depresses the conduction caused by electronic hopping between instable Ti^{3+} and Ti^{4+} and between Eu^{3+} and metastable Eu^{2+}. Therefore, C-BE5T exhibits a significantly lower dielectric loss (<0.03) at temperatures less than 140 °C.

4.3. Effect of the microstructure, Eu^{2+}/Eu^{3+} ions, and Mn^{2+} impurities on the dielectric properties of C-BE5T

The maximum permittivity (ε'_m) and average grain size (g) of BET increases with increasing T_s (Fig. 5). A relationship apparently exists between g and ε'_m. A decrease in ceramic porosity is well known to increase dielectric permittivity [5]. The variations in ε'_m and in the ceramic density (ρ) as a function of T_s for BE5T are depicted in Fig. 11. When $T_s\leq 1350$ °C, the parallel relationship between the ε'_m–T_s and the ρ–T_s curves demonstrates that, with increasing T_s, a decrease in ceramic porosity, in addition to the grain size, plays a predominant role in the increase in permittivity. The ceramic density is nearly constant for $T_s\geq 1350$ °C, and the increase in ε'_m with increasing T_s is consistent with the increase in g with increasing T_s. However, we hypothesize that an exaggerated grain growth in C-BE5T is not the main reason for obtaining the highest ε'_m among all of the BE5T ceramics, but rather the common effect of both the $Eu_{Ba}^{3+}-Ti_{Ti}^{3+}$ complexes and the dynamic equilibrium in Eq. (5) is responsible for the high-k behavior in C-BE5T: this hypothesis is discussed further in the following paragraph.

The T_m of BE5T decreases linearly with T_s at a rate of −0.46 °C/K (Fig. 5 inset), which is equivalent to a dramatic rate of −21 °C/at% Eu for C-BE5T. This rate is analogous to that caused by La^{3+} [26] and Ce^{3+} [27] doping at Ba sites.

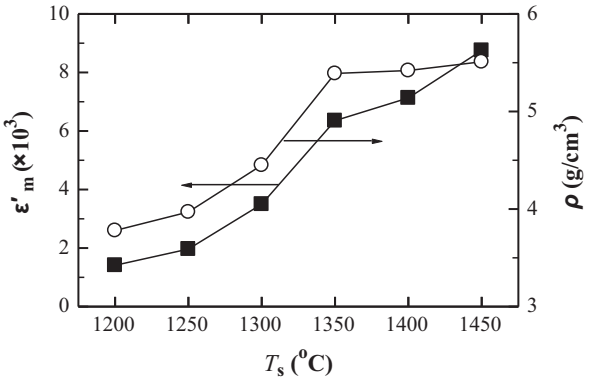

Fig. 11. Variations in ε'_m and in the ceramic density (ρ) as a function of T_s for BE5T.

On the basis of the XPS results for $(Ba_{1-x}Eu_x)TiO_3$ synthesized under high pressure and temperature [23], a reasonable assumption is made that the concentrations of Eu^{2+} and Eu^{3+} in C-BE5T are identical (2.5%). The ionic radius of Eu^{2+} (1.43 Å) is the same as that of Sr^{2+} (1.44 Å). Strontium doping in $BaTiO_3$ induces a very low peak-shifting rate of −3 °C/at% Sr [28,29]. The Eu^{2+} ions are therefore most likely not responsible for the rapid peak-shifting rate.

The rapid peak-shifting rate in C-BE5T is mainly due to the common effect of both the $Eu_{Ba}^{3+}-Ti_{Ti}^{3+}$ complex and the dynamic equilibrium shown in Eq. (5). In detail, the dynamic equilibrium shown in Eq. (5) can make Eu^{3+}/Eu^{2+} in C-BE5T exhibit the nature of Eu^{3+} because of the dual character of Eu ions. With an increase in T_s, the increase in the Eu^{3+} concentration causes a rapid decrease in T_m and an increase in ε'_m. In addition, the existence of the mixed valence of Ti^{4+}/Ti^{3+} at Ti sites can accelerate the shift of the dielectric peak toward lower temperatures. This effect is similar to the case of $(Ba_{1-x}La_x)(Ti_{1-y-x/4}Ce_y)O_3$ [30].

Although a very strong Mn^{2+} sextet signal was observed in the EPR spectrum of C-BE5T, Mn impurities play an important role in depressing electronic conduction and further dielectric losses by trapping electrons in the ceramic. Manganese impurities are the background impurities. The concentration of Mn^{2+} impurities is so low (several ppm) that their effect on the dielectric permittivity can be neglected.

In summary, the low porosity, the dual character of mixed Eu^{2+}/Eu^{3+} ions, and the dynamic equilibrium in Eq. (5) are responsible for the high-k Y5V behavior of C-BE5T.

5. Conclusions

The sintering temperature (T_s) strongly affects the structure, dielectric and valence-state properties of $(Ba_{1-x}Eu_x)TiO_3$ ($x=0.05$) ceramics (BE5T). When $T_s\leq 1400$ °C, BE5T consists of the main tetragonal perovskite phase and a small amount of the $Eu_2Ti_2O_7$ pyrochlore phase. An increase in T_s leads to rapid grain growth. When T_s is increased to 1450 °C, a single-phase ceramic (C-BE5T) is formed, which exhibits a cubic structure, a course-grained feature (5.6 μm), a low dielectric loss (<0.03), and high-k Y5V behavior ($\varepsilon'_{RT}=8500$). The dielectric peak shifts rapidly toward low temperature with increasing T_s at a rate of −0.46 °C/K. The C-BE5T features a mixed valence of Eu^{2+}/Eu^{3+} rather than Eu^{2+} only. A dynamic equilibrium of $Eu_{Ba}^{3+}+Ti_{Ti}^{3+}\rightarrow Eu_{Ba}^{2+}+Ti_{Ti}^{4+}$ in C-BE5T is responsible for this rapid peak-shifting rate, low dielectric loss, and high-k diffuse phase transition that occurs near room temperature. An asymmetric main band at 2494 cm^{-1} and a weak sharp band at 1516 cm^{-1} are considered as a novel indication of cubic symmetry in C-BE5T. The dynamic equilibrium enables Eu ions to exhibit a dual character of both Eu^{2+} and Eu^{3+}.

Acknowledgments

This work was funded by the National Natural Science Foundation of China (21271084), the Projects of Jilin Provincial Science and Technology Department (20121825), and the International Science and Technology Cooperation (20110710).

References

[1] R. Pazik, D. Hreniak, W. Strek, V.G. Kessler, G.A. Seisenbaeva, Photoluminescence investigations of Eu^{3+} doped $BaTiO_3$ nanopowders fabricated using heterometallic tetranuclear alkoxide complexes, Journal of Alloys and Compounds 451 (2008) 557–562.

[2] M. García-Hernández, A. García-Murillo, F. de, J. Carrillo-Romo, D. Jaramillo-Vigueras, G. Chadeyron, E. De la Rosa, D. Boyer, Eu-doped $BaTiO_3$ powder and film from sol-gel process with polyvinylpyrrolidone additive, International Journal of Molecular Sciences 10 (2009) 4088–4101.

[3] R. Pazik, R.J. Wiglusz, W. Strek, Luminescence properties of $BaTiO_3$:Eu^{3+} obtained via microwave stimulated hydrothermal method, Materials Research Bulletin 44 (2009) 1328–1333.

[4] R. Reshmi, M.K. Jayaraj, K. Jithesh, M.T. Sebastia, Photoluminescence of Eu^{3+}-doped $Ba_{0.7}Sr_{0.3}TiO_3$ thin film for optoelectronic application, Journal of the Electrochemical Society 157 (2010) H783–H786.

[5] D.-Y. Lu, T. Koda, H. Suzuki, M. Toda, Structure and dielectric properties of Eu-doped barium titanate ceramics, Journal of the Ceramic Society of Japan 113 (2005) 721–727.

[6] D.-Y. Lu, X.-Y. Sun, M. Toda, Electron spin resonance investigations and compensation mechanism of europium-doped barium titanate ceramics, Japanese Journal of Applied Physics 45 (2006) 8782–8788.

[7] M.K. Rath, G.K. Pradhan, B. Pandey, H.C. Verma, B.K. Roul, S. Anand, Synthesis, characterization and dielectric properties of europium-doped barium titanate nanopowders, Materials Letters 62 (2008) 2136–2139.

[8] B.-E. Jun, E.J. Kim, Y.S. Kim, J.S. Kim, B.-C. Choi, B.K. Moon, J.H. Jeong, Dielectric and ferroelectric properties of $Eu_xBa_{1-x}TiO_3$ fine ceramics, Journal of the Korean Physical Society 53 (2008) 2659–2663.

[9] D.-Y. Lu, T. Ogata, H. Unuma, X.-C. Li, N.-N. Li, X.-Y. Sun, Self-compensation characteristics of Eu ions in $BaTiO_3$, Solid State Ionics 201 (2011) 6–10.

[10] Y. Mizuno, H. Kishi, K. Ohnuma, T. Ishikawa, H. Ohsato, Effect of site occupancies of rare earth ions on electrical properties in Ni-MLCC based on $BaTiO_3$, Journal of the European Ceramic Society 27 (2007) 4017–4020.

[11] T. Kolodiazhnyi, A. Petric, Analysis of point defects in polycrystalline $BaTiO_3$ by electron paramagnetic resonance, Journal of Physics and Chemistry of Solids 64 (2003) 953–960.

[12] T.D. Dunber, W.L. Warren, B.A. Tuttle, C.A. Randall, T. Tsur, Electron paramagnetic resonance investigation of lanthanide-doped barium titanate: dopant site occupancy, Journal of Physical Chemistry B 108 (2004) 908–917.

[13] D.-Y. Lu, M. Toda, T. Ogata, X.-Y. Sun, Point defect characteristics of high-k double rare-earth-doped $BaTiO_3$ ceramics with diffuse phase transition by electron spin resonance, Japanese Journal of Applied Physics 48 (2009) 021401.

[14] T.R.N. Kutty, P. Murugaraj, N.S. Gajbhiye, EPR evidence for activation of trap centers in PTCR $BaTiO_3$ ceramics, Materials Research Bulletin 20 (1985) 565–574.

[15] D.-Y. Lu, X.-Y. Sun, M. Toda, A novel high-k 'Y5V' barium titanate ceramics co-doped with lanthanum and cerium, Journal of Physics and Chemistry of Solids 68 (2007) 650–664.

[16] M. Kchikech, M. Maglione, Electron and lattice excitations in $BaTiO_3$-La, Journal of Physics: Condensed Matter 6 (1994) 10159–10170.

[17] P.S. Dobal, A. Dixit, R.S. Katiyar, Z. Yu, R. Guo, A.S. Bhalla, Micro-Raman study of $Ba_{1-x}Sr_xTiO_3$ ceramics, Journal of Raman Spectroscopy 32 (2001) 147–149.

[18] M.C. Chang, S.C. Yu, Raman study for $(Ba_{1-x}Ca_x)TiO_3$ and $Ba(Ti_{1-y}Ca_y)O_3$ crystalline ceramics, Journal of Materials Science Letters 19 (2000) 1323–1325.

[19] Z.Z. Lazarevic, M.M. Vijatovic, B.D. Stojanovic, M.J. Romcevic, N.Z. Romcevic, Structure study of nanosized La- and Sb-doped $BaTiO_3$, Journal of Alloys and Compounds 494 (2010) 472–475.

[20] R. Farhi, M. El Marssi, A. Simon, J. Ravez, A Raman and dielectric study of ferroelectric $BaTi_{1-x}Zr_xO_3$ ceramics, European Physical Journal B 9 (1999) 599–604.

[21] A. Dixit, S.B. Majumder, P.S. Dobal, R.S. Katiyar, A.S. Bhalla, Phase transition studies of sol-gel deposited barium zirconate titanate thin films, Thin Solid Films 447–448 (2004) 284–288.

[22] M. Deluca, C.A. Vasilescu, A.C. Ianculescu, D.C. Berger, C.E. Ciomaga, L.P. Curecheriu, L. Stoleriu, A. Gajovic, L. Mitoseriu, C. Galassi, Investigation of the composition-dependent properties of $BaTi_{1-x}Zr_xO_3$ ceramics prepared by the modified Pechini method, Journal of the European Ceramic Society 32 (2012) 3551–3566.

[23] D.-Y. Lu, M. Sugano, X.-Y. Sun, W.-H. Su, X-ray photoelectron spectroscopy studies on $Ba_{1-x}Eu_xTiO_3$, Applied Surface Science 242 (2005) 318–325.

[24] L.P. Yurchenko, A.M. Slipenyuk, M.D. Glinchuk, I.P. Bykov, V.A. Mikheev, V.D. Tkachenko, E.P. Garmash, Impurities in perovskites: evidence from ESR of posistor barium titanate ceramics, Ferroelectrics 288 (2003) 235–241.

[25] G.A. Samara, The relaxational properties of compositionally disordered ABO_3 perovskites, Journal of Physics: Condensed Matter 15 (2003) R367–R411.

[26] F.D. Morrison, D.C. Sinclair, J.M.S. Skakle, A.R. West, Novel doping mechanism for very-high-permittivity barium titanate ceramics, Journal of the American Ceramic Society 81 (1998) 1957–1960.

[27] J.H. Hwang, Y.H. Han, Dielectric properties of $(Ba_{1-x}Ce_x)TiO_3$, Japanese Journal of Applied Physics 39 (2000) 2701–2704.

[28] L. Szymczak, Z. Ujma, J. Hańderek, J. Kapusta, Sintering effects on dielectric properties of $(Ba,Sr)TiO_3$ ceramics, Ceramics International 30 (2004) 1003–1008.

[29] C.L. Fu, C.R. Yang, H.W. Chen, Y.X. Wang, L.Y. Hu, Microstructure and dielectric properties of $Ba_xSr_{1-x}TiO_3$ ceramics, Materials Science and Engineering B 119 (2005) 185–188.

[30] D.-Y. Lu, M. Sugano, M. Toda, High-permittivity double rare earth-doped barium titanate ceramics with diffuse phase transition, Journal of the American Ceramic Society 89 (10) (2006) 3112–3123.